SCATTERING PROPERTIES OF ORIENTED HEXAGONAL ICE CRYSTALS

A Thesis

by

FENG ZHANG

Submitted to the Office of Graduate Studies of
Texas A&M University
in partial fulfillment of the requirements for the degree of

MASTER OF SCIENCE

August 2009

Major Subject: Atmospheric Sciences

SCATTERING PROPERTIES OF ORIENTED HEXAGONAL ICE CRYSTALS

A Thesis

by

FENG ZHANG

Submitted to the Office of Graduate Studies of
Texas A&M University
in partial fulfillment of the requirements for the degree of

MASTER OF SCIENCE

Approved by:

Chair of Committee,	Ping Yang
Committee Members,	Thomas Wilheit
	George Kattawar
Head of Department,	Kenneth Bowman

August 2009

Major Subject: Atmospheric Sciences

ABSTRACT

Scattering Properties of Oriented Hexagonal Ice Crystals. (August 2009)

Feng Zhang, B.S., Nankai University;

M.S., Nankai University;

M.S., Texas A&M University

Chair of Advisory Committee: Dr. Ping Yang

To interpret the data from spaceborn lidar measurements, one must have a basic understanding of the backscattering of oriented ice particles. The conventional ray-tracing method is not applicable to the scattering of light by oriented particles. In this study, the dipole approximation (DDA) method is employed to the scattering of light on oriented hexagonal ice columns and plates with various tilting angles. It is found that the oriented hexagonal ice particles tend to have strong backscattering intensity with low depolarization ratios which are strongly dependant on the tilting angle of oriented particles. The present results show that the effect of particle orientation plays an important role in determining the optical properties of ice clouds consisting of horizontally oriented ice crystals.

To My Parents

ACKNOWLEDGMENTS

I would like to thank Dr. Ping Yang, my supervisor, for his instruction and constant support during this research.

I would also like to thank my committee members. Their valuable feedback helped me to improve the thesis in many ways.

The members of Dr. Yang's group contributed immensely to my personal and professional time. The group has been a source of friendship and have provided good advice and collaboration.

Last but not least, I thank my family for always being there when I needed them most, and for supporting me through all these years.

TABLE OF CONTENTS

LIST OF FIGURES

FIGURE Page

CHAPTER I

INTRODUCTION

Cirrus clouds cover more than 20% of the globe [1]. Mainly composed of ice crystals, cirrus clouds located in the upper troposphere play an important role in the earth's climate system [2, 3]. To fully understand the impact of clouds on the climate system, detailed information about cloud properties, height, temperature and phase must be known. Due to the high altitude and large scale of cirrus clouds, satellite based remote sensing is often employed to detect these properties [4].

CALIPSO (Cloud-Aerosol Lidar and infrared Pathfinder Satellite Observations) is a joint effort satellite mission between NASA and CNES, and aimed at improving our knowledge of the role of aerosols and clouds in climate systems [5]. The primary instrument on CALIPSO, the Cloud-Aerosol Lidar with the Orthogonal Polarization (CALIOP), is a dual wavelength lidar designed to acquire the vertical profiles of backscatter at wavelengths of 532 nm and 1064 nm. Research into cloud-climate feedback utilizes the information retrieved by CALIOP combined with data from other "A-Train" satellites to study the relationships between cloud phase, cloud height and cloud optical thickness. The 532 nm channel of CALIOP has dual polarization and reports the linear depolarization ratio [5]. The cloud phase can be determined from the relationship between the lidar depolarization ratio and the effective backscatter.

Hu et al.[6] proposed a method to discriminate the cloud phase based on the depolarization ratio-effective lidar ratio relation derived from the spaceborn lidar cloud data. In his paper, layer-integrated depolarization ratio δ and layer-integrated

---

The journal model is Applied Optics.

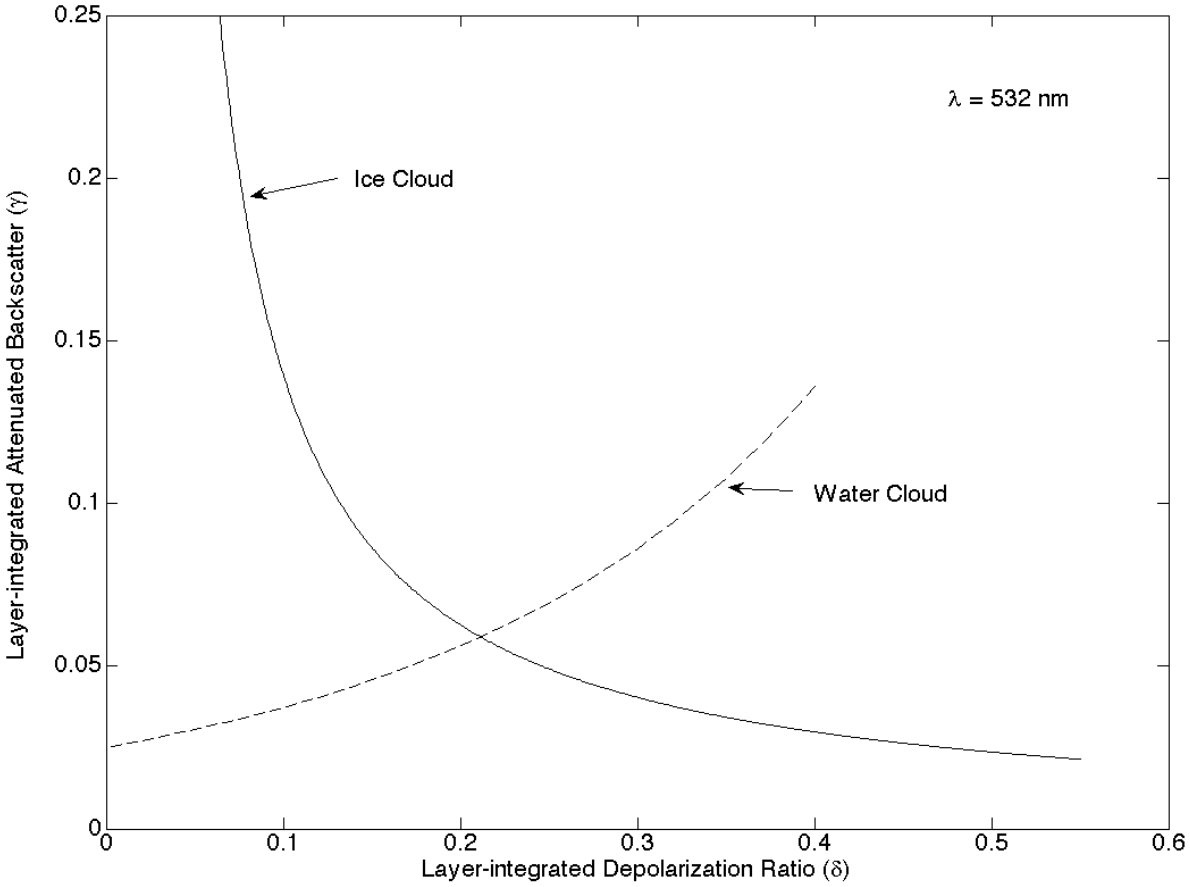

Fig. 1. Schematic curves showing the relationship between integrated depolarization ratio and integrated attenuated backscatter derived by Hu[7].

attenuated backscatter γ are defined as [7]:

$$\delta = \int_{top}^{base} \beta'_{\perp}(r)dr \Big/ \int_{top}^{base} \beta'_{//}(r)dr \tag{1.1}$$

$$\gamma' = \int_{top}^{base} (\beta_{\perp} + \beta_{//})dr \tag{1.2}$$

Hu et al. [7] derived the relationship between CALIPSO lidar δ and γ for both ice and water clouds based on the data similar to those shown in Fig. 1 and 2.

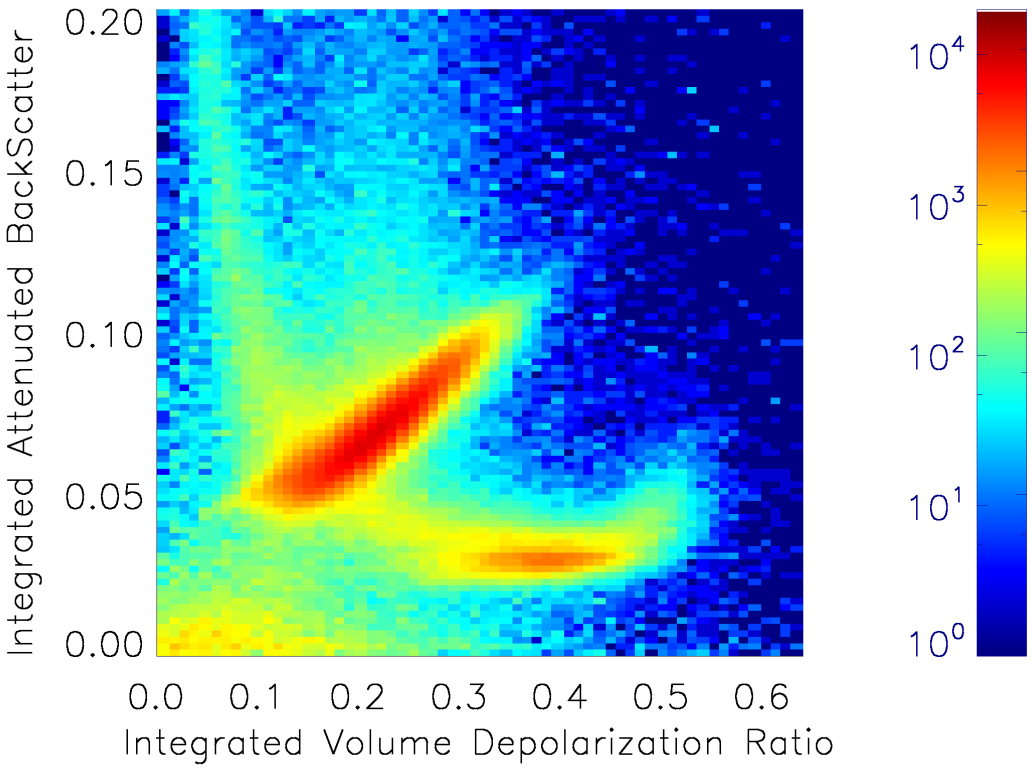

Fig. 2. The relationship between integrated depolarization ratio and integrated attenuated backscatter shown by CALIPSO DATA. [Courtesy of Jianxu Lu].

For water clouds composed of spherical water droplets, δ increases as γ increases. For ice clouds, δ decreases as γ increases [8, 9]. It should be noted that the single scattering process by water droplets does not depolarize the backscattered light, but multiple scattering in water clouds tends to lead to a large depolarization ratio in the backscattering direction. The lower part of the ice cloud curve in Fig. 1 corresponds to the randomly oriented ice crystals in the cloud. The upper left branch of the ice cloud curve corresponds to high backscatter values and low depolarization ratios, which are generally believed to be associated with zenith enhanced backscatter (ZEB) from horizontally oriented particles in ice clouds. Many lidar experiments have observed zenith enhanced backscatter from cirrus clouds at the zenith angle [10]. The ZEB signature is found to be extremely strong when the lidar is pointed directly at the zenith and decreases quickly when the lidar beam direction is slightly tilted off the zenith. The measured depolarization ratio of ZEB is approximately zero, because, while the lidar beam is focused directly downward, the two horizontally placed faces have a strong effect on backscatter, but the parallel and perpendicular components of the electric field of the incident lidar beam are indistinguishable and the backscattered light has a very small depolarization ratio. The existence of horizontally oriented ice crystals has been confirmed by several lidar observations [11, 12, 13]. Furthermore, observations by the Polarization and Directionality of the Earth's Reflectances (POLDER) instrument have found that approximately 40% of the ice crystals in cirrus clouds are horizontally oriented [14]. However, in order to fully understand the relationship between depolarization ratio-effective lidar ratio, a detailed analysis of the backscattering properties of oriented hexagonal ice crystals is necessary.

CHAPTER II

METHODOLOGY

A. Basic scattering parameters

Using a spherical coordinate system associated with a right-handed Cartesian coordinate system with its origin at the observational point shown in Fig. 3, we can define the propagation direction of a plane electromagnetic wave with a unit vector **n**. In this spherical coordinate system, the unit vector **n** can be specified in terms of θ and ϕ. where θ in the range of $[0, \pi]$ is the azimuth angle and ϕ in the range of $[0, 2\pi]$is the zenith angle.

The equation of a plane electromagnetic wave in a medium with electric permittivity ϵ and magnetic permeability μ can be written as

$$\mathbf{E}(\mathbf{r}, t) = \mathbf{E} e^{(i\mathbf{k}\cdot r - i\omega t)} \tag{2.1}$$

where k is the wave vector. **E** can be decomposed into two components E_θ and E_ϕ. E_θ lies in the meridional plane defined by **n** and the z axis. E_ϕ is perpendicular to this plane.

The Stokes parameters are defined as [15]:

$$\mathbf{I} = \begin{bmatrix} I \\ Q \\ U \\ V \end{bmatrix} = \sqrt{\frac{\epsilon}{\mu}} \begin{bmatrix} E_\theta E_\theta^* + E_\phi E_\phi^* \\ E_\theta E_\theta^* - E_\phi E_\phi^* \\ -2\ Re\ E_\theta E_\phi^* \\ 2\ Im\ E_\theta E_\phi^* \end{bmatrix}. \tag{2.2}$$

From the definition we can see that each component of the Stokes parameters is a real quantity. The Stokes parameters have the dimension of energy flux so they can

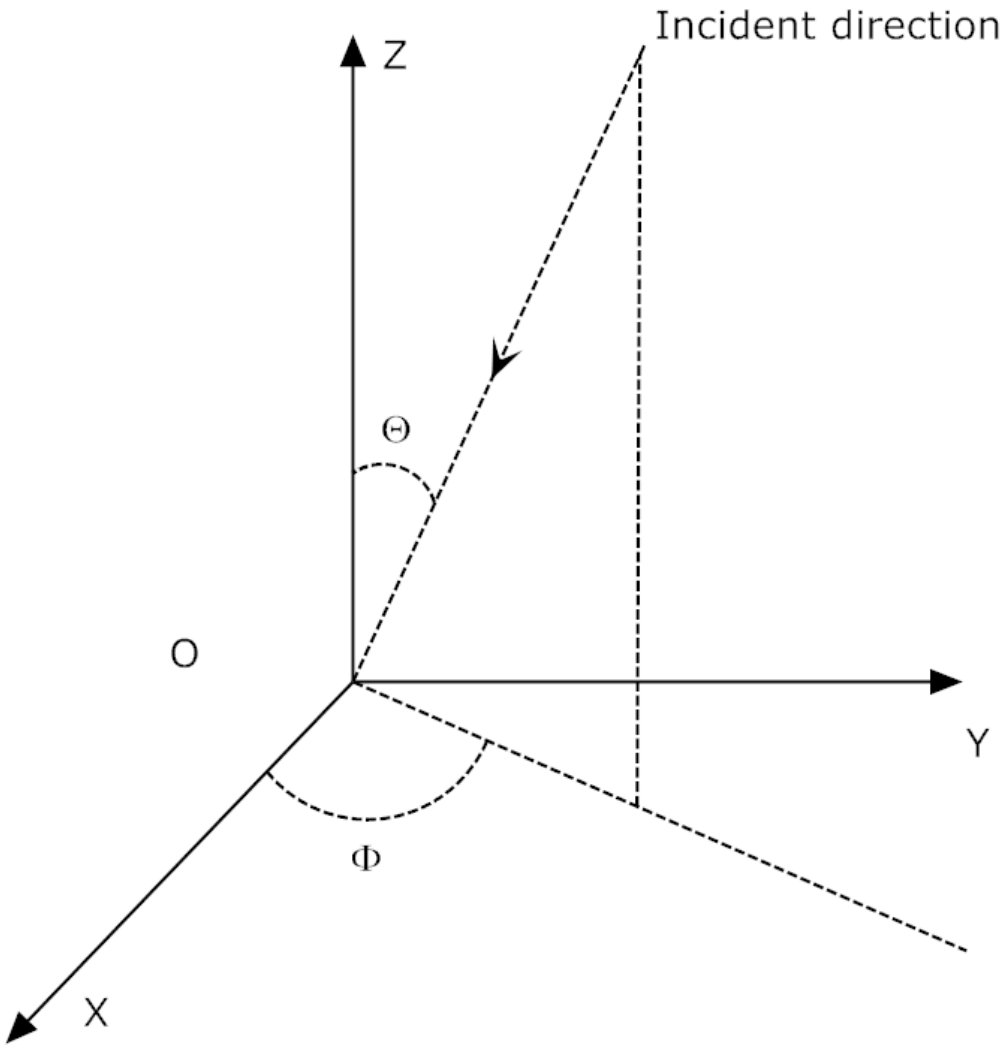

Fig. 3. The spherical coordinate system associated with a right-handed Cartesian coordinate system.

be directly measured by optical instruments.

The Stokes parameters associated with the scattering field can be linked to those of the incident field by a linear transformation.

$$\begin{pmatrix} I_s \\ Q_s \\ U_s \\ V_s \end{pmatrix} = \begin{pmatrix} P_{11} & P_{12} & P_{13} & P_{14} \\ P_{21} & P_{22} & P_{23} & P_{24} \\ P_{31} & P_{32} & P_{33} & P_{34} \\ P_{41} & P_{42} & P_{43} & P_{44} \end{pmatrix} \begin{pmatrix} I_i \\ Q_i \\ U_i \\ V_i \end{pmatrix} \tag{2.3}$$

The degree of polarization (DP), degree of linear polarization (DLP) and the degree of circular polarization (DCP) are defined as follows [16]:

$$DP = \frac{\sqrt{P_{21}^2 + P_{31}^2 + P_{41}^2}}{P_{11}} \tag{2.4}$$

$$DLP = -\frac{P_{21}}{P_{11}} \tag{2.5}$$

$$DCP = -\frac{P_{41}}{P_{11}} \tag{2.6}$$

$$\tag{2.7}$$

If the laser beam is linear polarized, the linear depolarization ratio can be written as:

$$\delta_L = \frac{P_{11} + P_{12} - P_{21} - P_{22}}{P_{11} + P_{12} + P_{21} + P_{22}}. \tag{2.8}$$

In our current research, the lidar beam on CALIPSO is linearly polarized, thus we only need to consider the linear depolarization ratio and the degree of linear polarization.

B. The discrete dipole approximation

For scatters such as hexagonal plates, an exact solution of Maxwell's equations is difficult to obtain and numerical methods are preferred. The conventional geometric

optics method (GOM) is not applicable to oriented particles because of its inherent limits [16]. Specifically, the phase function derived from the GOM is the superposition of the diffraction contribution and two delta functions, therefore, more rigorous numerical methods must be applied.

The discrete dipole approximation (DDA) introduced by Purcell and Pennypacker [17] is a widely used method for computing the electromagnetic wave scattering problems for particles with arbitrary shapes and composition. The general premise of the DDA is to replace a scatter with a number of dipoles which interact with both the incident field and each other. The interaction between dipoles is governed by a system of linear equations. The dipole polarizations are obtained by solving the linear equations, and the measurable scattering properties can be derived from these dipole polarizations. Goedecke and O'Brien [18] demonstrated that the DDA can be derived from the volume integral equation for the electric field by dividing the scatter into a set of small sub-volumes. The final equation produced by the integral equation is essentially the same as the one used for the discrete dipole approximation.

Following Purcell's original hypothesis, suppose we have a scatter with the incident field $\mathbf{E}_{inc}$, and we can divide the scatter into a set of dipoles $\mathbf{x_i}, i = 1, 2...., N$ with polarizabilities tensor a_i. Each dipole's polarization is $\mathbf{P}_i = a_i \mathbf{E}_i$, where $\mathbf{E}_i$ is the sum of incident field $\mathbf{E}_{inc,i}$ and the fields contributed by all the other dipoles.

$$\mathbf{E}_i = \mathbf{E}_{inc}, i - \sum_{j \neq i} \mathbf{A}_{ij} \mathbf{P}_j, \tag{2.9}$$

where $\mathbf{A}_{ij}\mathbf{P}_j$ is the field on dipole $\mathbf{x}_i$ induced by dipoles $\mathbf{P}_j$ including retardation effects. Each $\mathbf{A}_{ij}$ is a 3×3 matrix given by [19]:

$$\mathbf{A}_{ij} = \frac{exp^{ikr_{ij}}}{r_{ij}} \times \left[k^2(\hat{r}_{ij}\hat{r}_{ij} - I_3) + \frac{ikr_{ij} - 1}{r_{ij}^2}(3)(\hat{r}_{ij}\hat{r}_{ij} - I_3) \right], \tag{2.10}$$

If we define $\mathbf{A}_i i = a_j^{-1}$, the problem is reduced to solve $3N$ complex linear equations

for $\mathbf{P}_j$:

$$\sum_{j=1}^{N} \mathbf{A}_{ij}\mathbf{P}_j = \mathbf{E}_{inc,i}. \tag{2.11}$$

The major physics problem in the DDA formulation is to assign the dipole polarizabilities to the dipoles in the scatter. The original study by Purcell and Pennypacker used the Clausius-Mossotti polarizability [17]:

$$a_j^{CM} = \frac{3d^3}{4\pi}\frac{\epsilon - 1}{\epsilon + 2}, \tag{2.12}$$

where $\epsilon = m^2$ is the complex dielectric function of the scatter at position r.

The absorption and extinction cross section can be directly calculated from the internal fields [19]:

$$C_{abs} = \frac{4\pi k}{|E_0|^2}\sum_{j=1}^{N}(Im(P_j \cdot (a_j^{-1})^* P_j^*) - \frac{2}{3}k^3|P_j|^2), \tag{2.13}$$

$$C_{ext} = \frac{4\pi k}{|E_0|^2}\sum_{j=1}^{N} Im(E_{inc,j}^* \cdot \mathbf{P}_j). \tag{2.14}$$

The scattering cross section $C_{sca} = C_{ext} - C_{abs}$.

Efforts have been made to improve the DDA since the original paper of Purcell and Pennypacker. It has been noted by Draine [20, 21] that the Clausius-Mossotti polarizability does not satisfy energy conservation, which in turn fails at optical theorem. A correction to the polarizability for a finite dipole was proposed based on the radiative reaction relation [**?**]:

$$\alpha^{RR} = \frac{\alpha^{CM}}{1 - \frac{2}{3}ik^3\alpha^{CM}} \tag{2.15}$$

In order to get the correct phase of the scattered electromagnetic wave, we need to make sure that the phase change between two adjoining dipoles is less than 1 rad.

Thus one can get the following criterion of DDA [19]:

$$|m|kd \leq 1, \tag{2.16}$$

where m is the refractive index, k is the wave number, and d is the dipole size.

It is well known that the errors in the DDA are mainly due to two factors: the shape of the scatter, and the discretization of the scatter. The first error arises because the particle shape may not always be described exactly by a set of sub-volumes. To reduce the shape errors, adaptive discretization can be employed, which uses different dipole sizes to get a better fit of the scatter shape. The second error is due to the finite size of each cell and can be reduced by choosing a different dipole polarizability formula. The DDA code we used in our research is called ADDA, developed by Yurkin, et al. [23, 24, 25].

C. T-matrix method

The T-matrix approach proposed by Waterman [26] is based on the orthogonal vector spherical wave function expansion of the incident and scattered electric field vectors.

$$E^{inc}(R) = \sum_{n=1}^{\infty} \sum_{m=-n}^{n} [a_{mn} RgM_{mn}(kR) + b_{mn} RgN_{mn}(kR)] \tag{2.17}$$

$$E^{sca}(R) = \sum_{n=1}^{\infty} \sum_{m=-n}^{n} [c_{mn} RgM_{mn}(kR) + d_{mn} RgN_{mn}(kR)] \tag{2.18}$$

where a_{mn}, b_{mn}, c_{mn} and d_{mn} are the coefficients and are complex numbers. $M_{mn}$and N_{mn} are vector spherical wave functions of the degree n and the order m. Because of the linearity of Maxwell's equations, coefficients of the scattered field c_{mn} and d_{mn} can be linked to those of the incident field a_{mn} and b_{mn} via linear transformation

$$c_{mn} = \sum_{n\prime=1}^{\infty} \sum_{m\prime=-n\prime}^{n\prime} [T^{11}_{mnm\prime n\prime} a_{m\prime n\prime} + T^{12}_{mnm\prime n\prime} b_{m\prime n\prime}], \tag{2.19}$$

$$d_{mn} = \sum_{n\prime=1}^{\infty} \sum_{m\prime=-n\prime}^{n\prime} [T^{21}_{mnm\prime n\prime} a_{m\prime n\prime} + T^{22}_{mnm\prime n\prime} b_{m\prime n\prime}], \tag{2.20}$$

or in matrix form

$$\begin{bmatrix} c \\ d \end{bmatrix} = T \begin{bmatrix} a \\ b \end{bmatrix} = \begin{bmatrix} T^{11} & T^{12} \\ T^{21} & T^{22} \end{bmatrix} \begin{bmatrix} a \\ b \end{bmatrix}, \tag{2.21}$$

where we have suppressed the indices of each element. This is the basic equation of the T-matrix approach. In principle, the matrix, T, can be calculated with a standard method of calculating the scattering problem by particles, but the most commonly used method is the extended boundary condition method (**EBCM**)proposed by Barber and Yeh [27]. Mischenko [15] further developed this method and wrote a solid code to be made available to the public. A very important feature of the T-matrix method is that the T-matrix itself does not depend on either the propagation direction or polarization states of the incident and scattered waves. It only depends on the properties of the scatter, such as the shape, size and refraction index. A major advantage of the T-matrix method is that the T-matrix of a particle at a certain wavelength only need be calculated once and can then be used to calculate the scattering process for any orientation and polarization.

CHAPTER III

NUMERICAL RESULTS

Lidar experiments done by Platt et al. [30] on an altostratus cloud exhibited a layered structure possessing variable optical properties. The top layer of the cloud was characterized by high backscattering coefficients and very small depolarization ratios within the range of 0.03 to 0.05. The fundamental electromagnetic wave scattering theory indicates that spherically symmetrical and homogeneous scatters generate small depolarization ratios in the exact backscattering direction. The backscatter from ice crystals, with the contribution from internal reflection, is thought to generate large depolarization ratios. From electromagnetic wave theory, the main composition of the cloud top layer was classified as cloud droplets. The conclusion was supported by theoretical and experimental field studies [13]. Sassen [4] found the depolarization ratio of water clouds was near zero and of ice clouds approximately 0.5. As a result, the depolarization ratio was proposed as a tool to determine the cloud phase. It has been noted that spherical homogeneous particles are not the only scatters that generate strong backscattering and low depolarization ratios. Horizontally oriented ice crystal plates also have similar backscattering properties due to the specular reflection off two large basal faces as shown in Fig. 4. The conventional ray-tracing method fails for such scattering problem because it leads to singularities in the computation, specifically when dealing with the backscattered rays from the top and bottom surfaces. Therefore rigorous methods such as DDA or FDTD have to be applied.

A. Comparison between DDA and T-matrix.

In this section, both the T-matrix and the DDA methods are applied to oriented cylinders. By comparing the phase function obtained from both methods, the applicability

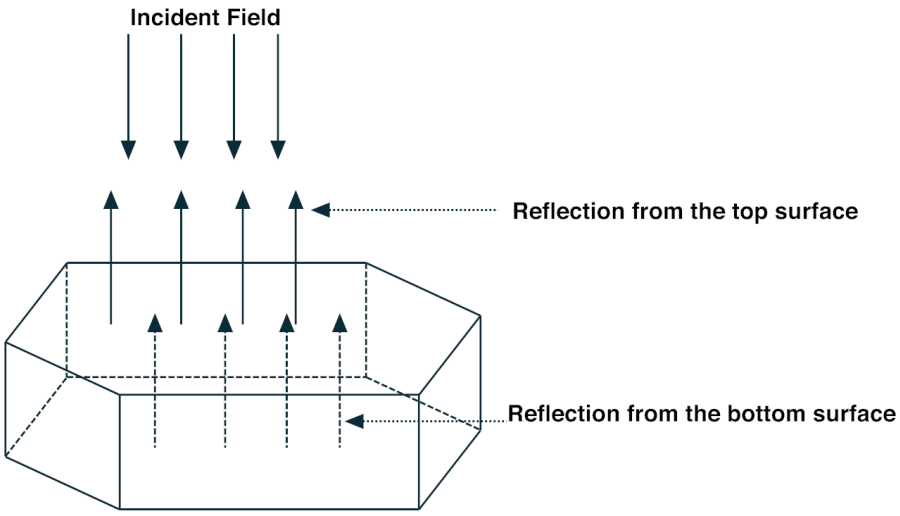

Fig. 4. The backscattering of hexagonal plate.

of DDA on oriented particles can be determined.

Usually for oriented particles, four angles: θ_i, ϕ_i, θ_s and ϕ_s are used to specify the scattering configuration. The incident angle θ_i and the azimuth angle ϕ_i define the incident direction in a laboratory coordinate system. The orientations of cylinders in the laboratory coordinate system are simplified by choosing the z axis as the symmetry axis of the two geometries [**?**].

The cylinder we used has the following properties: $D/L = 1$; the wavelength is $0.532\mu m$; and, the corresponding refractive index is $1.3117 + i2.6138 \times 10^{-9}$. The geometry of cylinder is shown in Fig. 5.

Fig. 6 shows the phase matrix element P_{11} calculated from both the T-matrix and the DDA methods with an incident angle of $\theta = 0^o$. From the figure we can clearly see that there is little difference between the results obtained from the DDA and T-matrix methods at all scattering angles. Excellent agreement can be found at the backscattering direction $\theta = 180^o$. Here we should notice the ripple structure of the phase function, pointed out by Mischenko [28], which is mainly due to the interference between the reflected fields from the two parallel surfaces of the particle. Such interference is related to the particle size parameter and can be smoothed out if the phase function is integrated over certain particle size distribution.

Figs. 7, 8 and 9 show P_{12}/P_{11}, P_{33}/P_{11} and P_{43}/P_{11} computed from both the T-matrix and DDA methods, and we can see that they agree very well in the forward and back scattering directions. We also notice that there is some discrepancy at around 90 degrees. This is mainly due to the sharp edge of the cylinder because the T-matrix method approximates the electric field in terms of spherical vector wave functions.

In general, we can see that the results from the T-matrix and DDA methods agree very well for non-spherical particles such as cylinders. The comparison illustrates

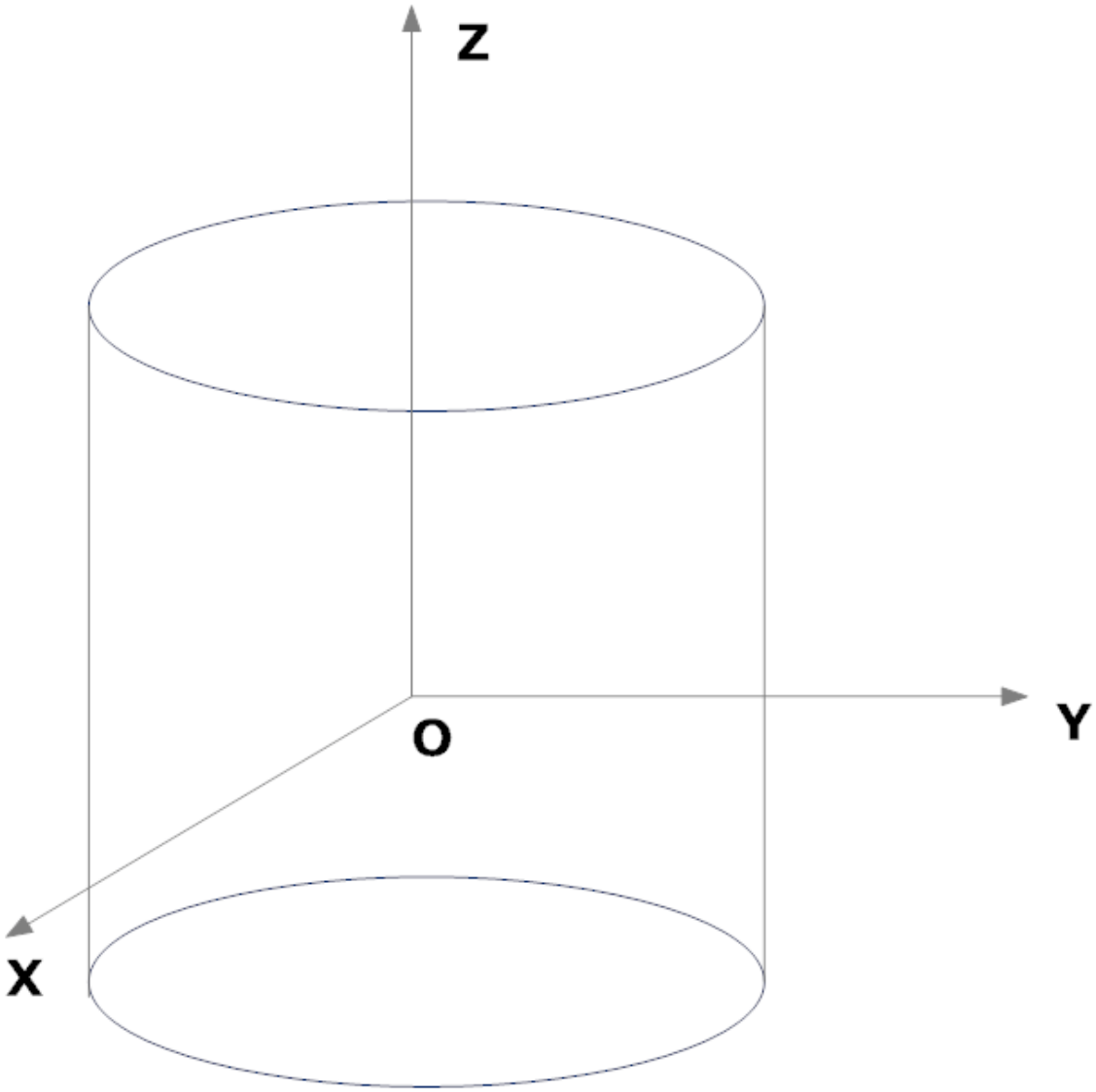

Fig. 5. The geometry of cylinder.

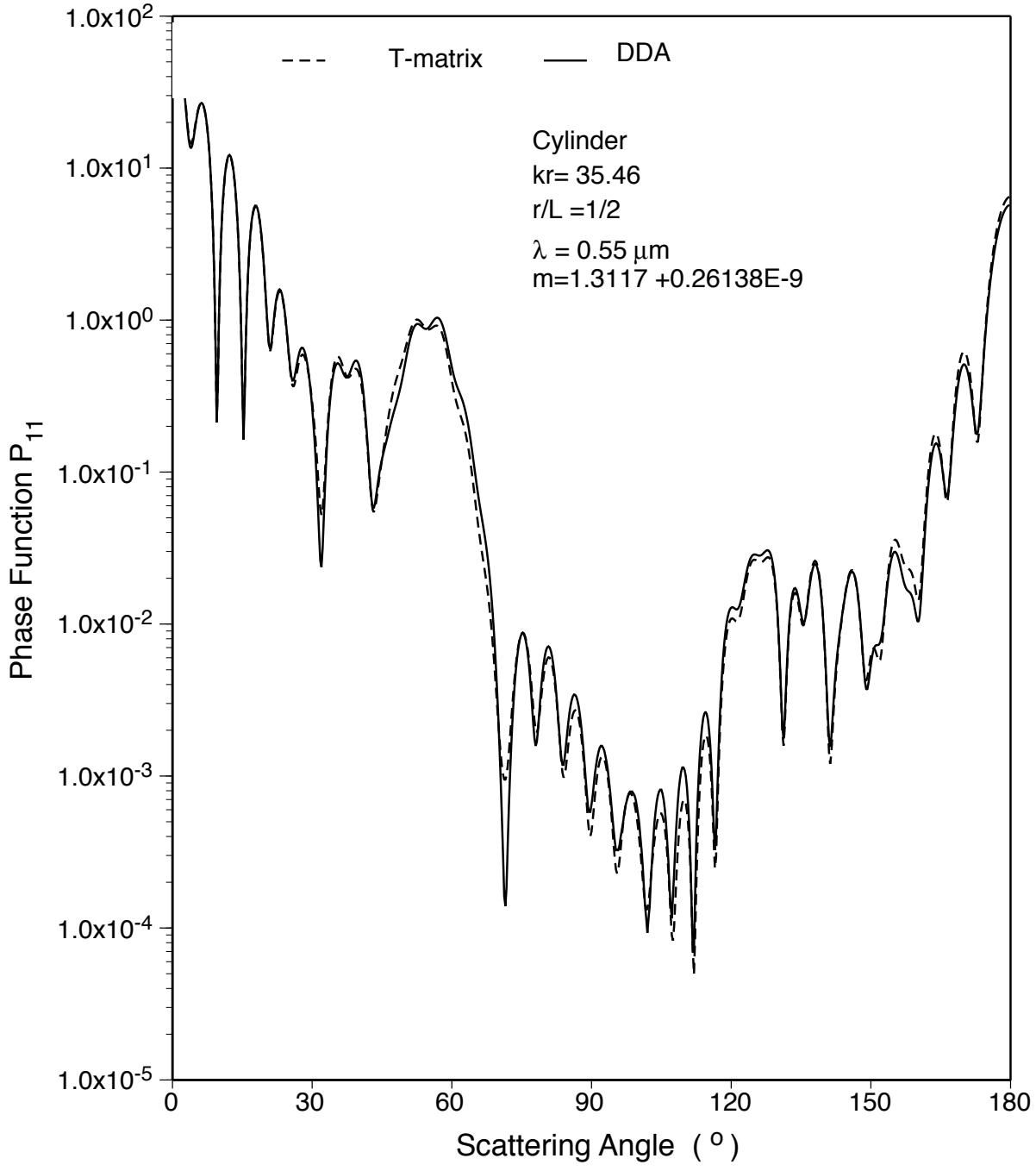

Fig. 6. Phase function from the T-matrix and DDA methods for a cylinder with incident angle $\theta = 0^o$.

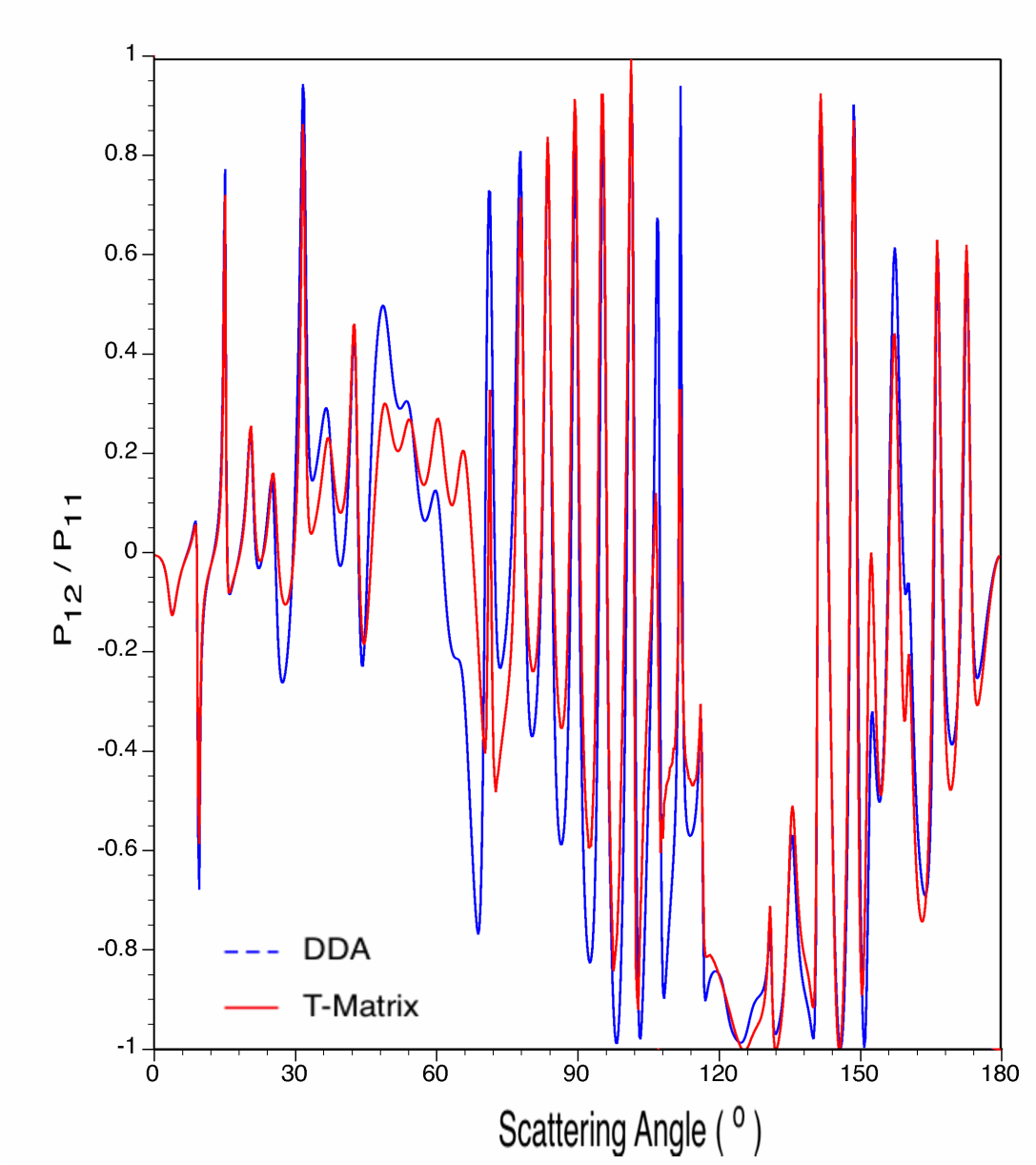

Fig. 7. P_{12}/P_{11} from the T-matrix and DDA methods for a cylinder with incident angle $\theta = 0^o$.

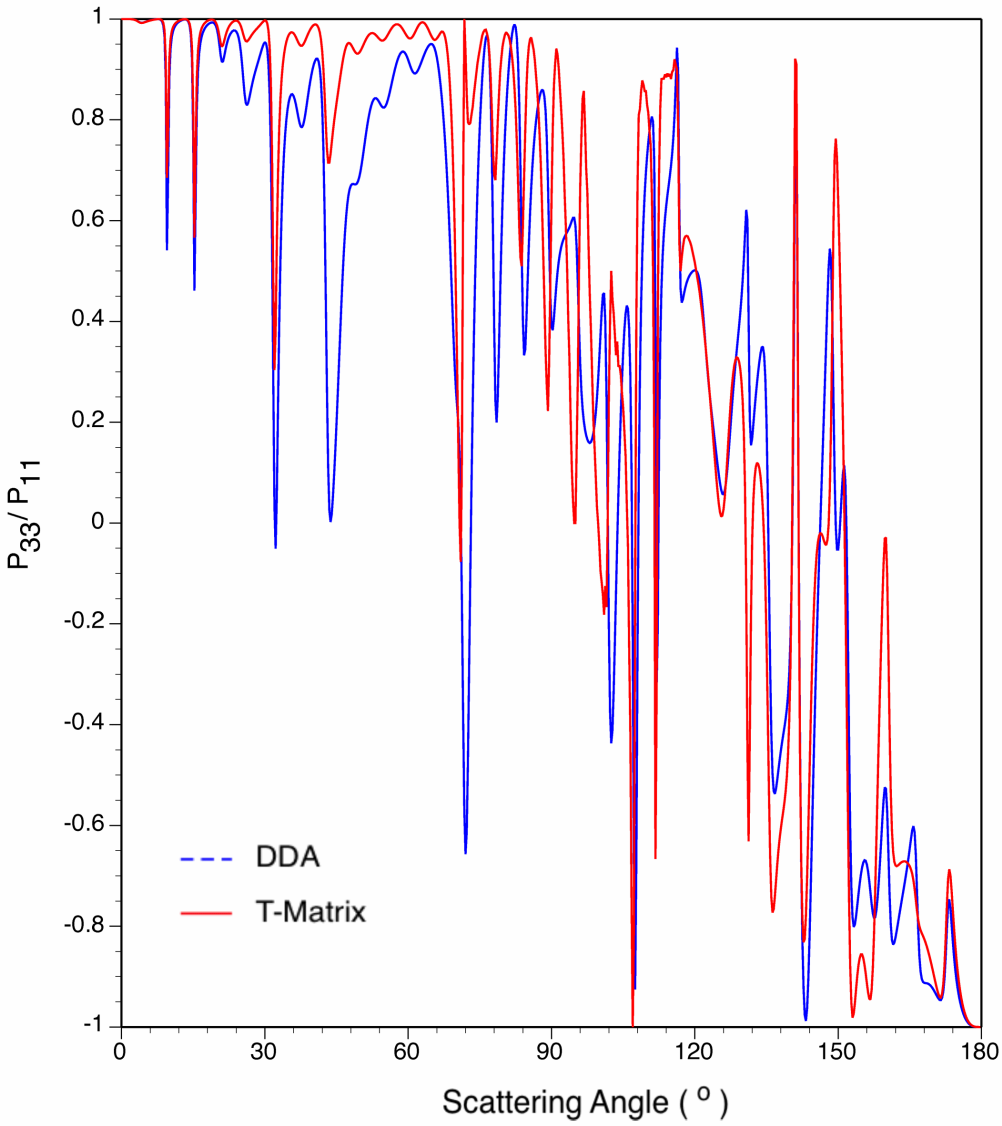

Fig. 8. P_{33}/P_{11} from the T-matrix and DDA methods for a cylinder with incident angle $\theta = 0^o$.

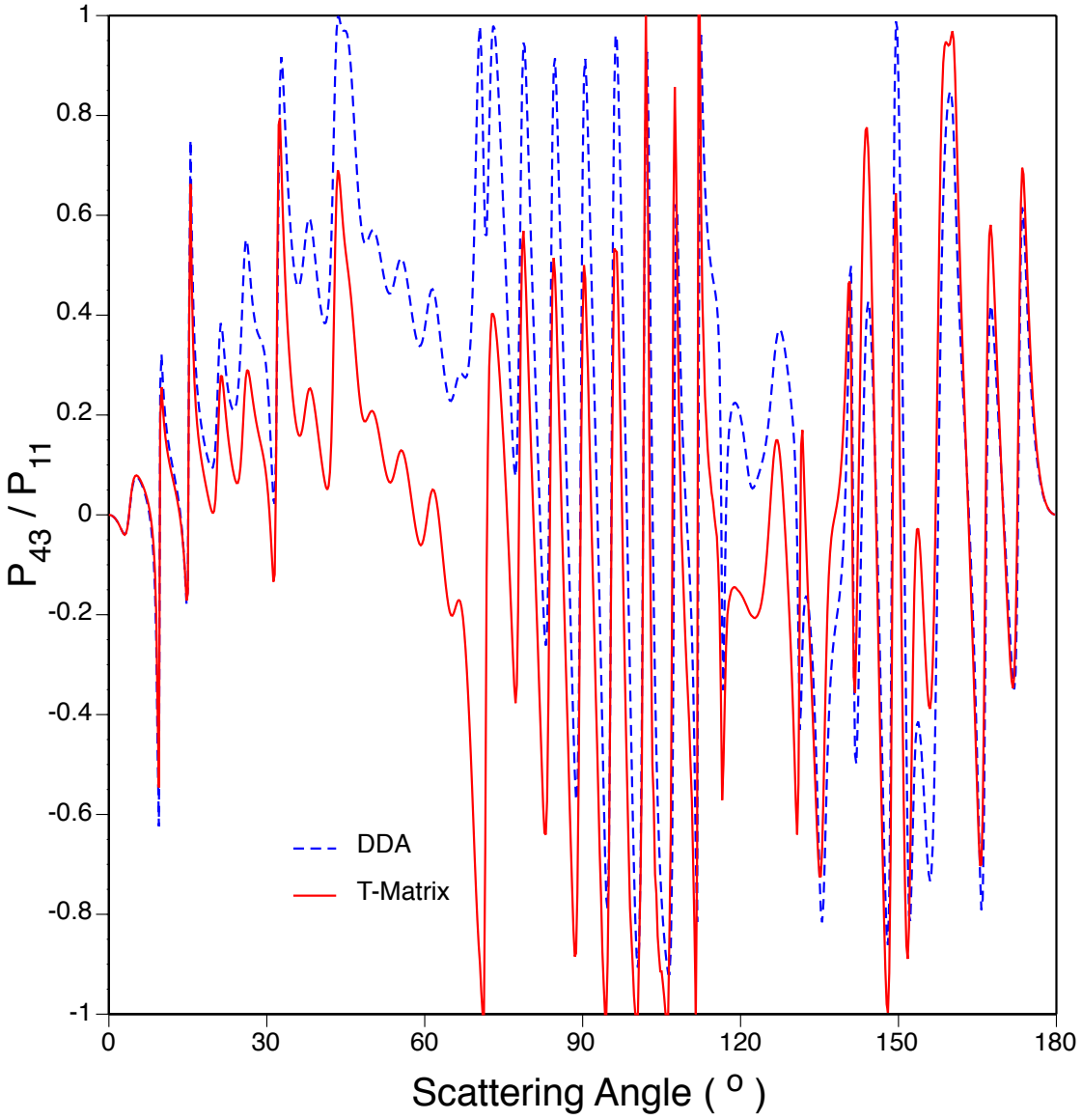

Fig. 9. P_{43}/P_{11} from the T-matrix and DDA methods for a cylinder with incident angle $\theta = 0^o$.

that we can use the DDA method to study the scattering properties of non-spherical particles.

B. Application to hexagonal ice plates and columns

Hexagonal prisms are the basic structure of ice crystals in cirrus clouds. Hexagonal prisms can be totally defined with terms of its side length a and length L. The aspect ratio of hexagonal prism is defined as 2a/L. When the aspect ratio is larger than 1, this geometry is a hexagonal plate in which size parameter is defined as ka, where k is the wave number given by $k = 2\pi/\lambda$. When the aspect ratio is smaller than 1, the geometry becomes a hexagonal column with size parameter kL. Fig. 10 and 11 show the geometry of hexagonal plates and hexagonal columns.

Hexagonal ice plates grow in the temperature range from -8 to -25°$C$with the largest growth rate occurring in the range from -12 to -15°C [29]. The plate grows in three dimensions until its short axis reaches maximal length, after which the growth occurs mainly along the long axis . In air, the hexagonal ice plates will fall while having their longest axis parallel to the horizontal plane due to the mechanical stability of the system. When the lidar beam is pointing directly downwards, the basal faces produce specular reflection.

We use the following relationship [30] for the ice plates involved in this study.

$$L = 2.4883a^{0.474}, \quad 5\mu m \leq a \leq 1500\mu m, \tag{3.1}$$

where a is the semi-width of the cross section and L is the thickness of the plate.

Fig. 12 shows the phase matrix element of a hexagonal plate. The incident direction is perpendicular to the top basal face of the plate. There is strong backscatter in the backscattering direction ($\theta = 180^o$). It should be noted that, like cylinders,

there are also ripples as the scattering angle θ varies from 0^o to 180^o. The ripples are caused by the interference between the reflected rays from the two basal faces of the plate. It should also be noticed that the phase function is periodical with respect to ϕ which is caused by the symmetry of the hexagonal plates with the Z axis.

In this study, we chose the aspect ratio 3 for hexagonal plates and 1/3 for columns.

Fig. 13 shows the phase function for the same plate but with an incident angle 3^o. We clearly see some deviation from Fig. 12, especially in the backscattering direction ($\theta = 180^o$).

Fig. 14 shows the phase function of a hexagonal column with an incident angle 0^o. The column has its longest axis and one of its side surfaces parallel to the horizontal plane. The phase function, in this case, is quite different from a horizontally oriented plate. While the phase matrix still shows strong backscattering at $\theta = 180^o$, the periodic behavior in the ϕ direction is suppressed because we only have mirror symmetry along the Z axis. The strong backscattering occurs because we have two relatively large side surfaces parallel to the horizontal plane causing strong reflections.

Fig. 15 shows the phase function of the same hexagonal column but with an incident angle 3^o. The phase function in this case shows some deviation from the previous direct incident case.

Fig. 16 and 17 show the backscattering cross section for incident angle 0^o and 3^o. As can be seen from the figures, the backscattering intensity is very sensitive to the incident angle.

Figs. 18 and 19 show the degree of linear depolarization for incident angle 0^o and 3^o. As can be seen from the figures. the degree of linear depolarization is not sensitive to the incident angle.

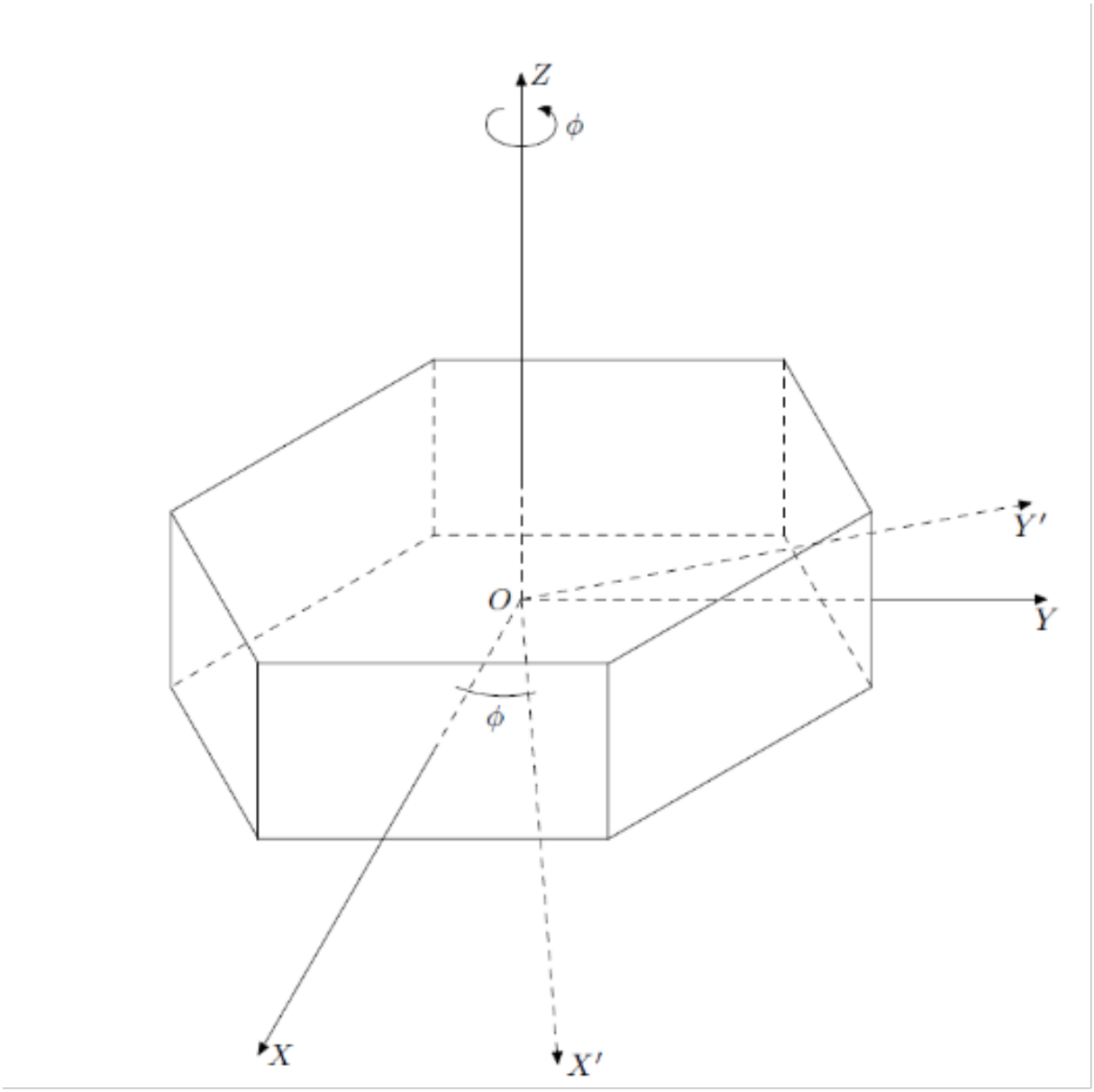

Fig. 10. The geometry for a hexagonal ice plate.

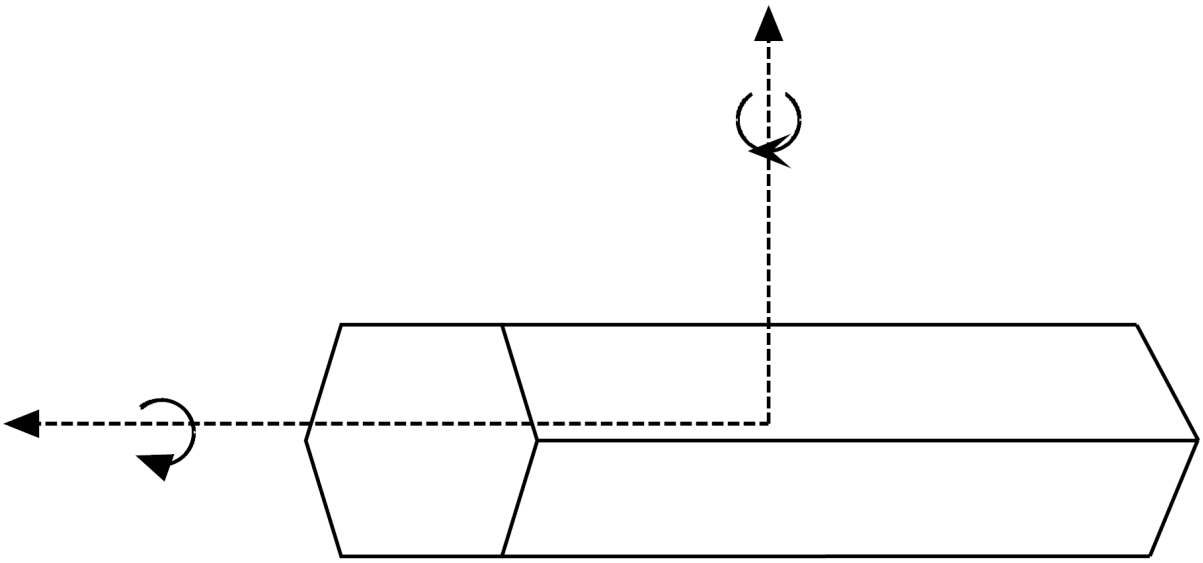

Fig. 11. The geometry for a hexagonal ice column.

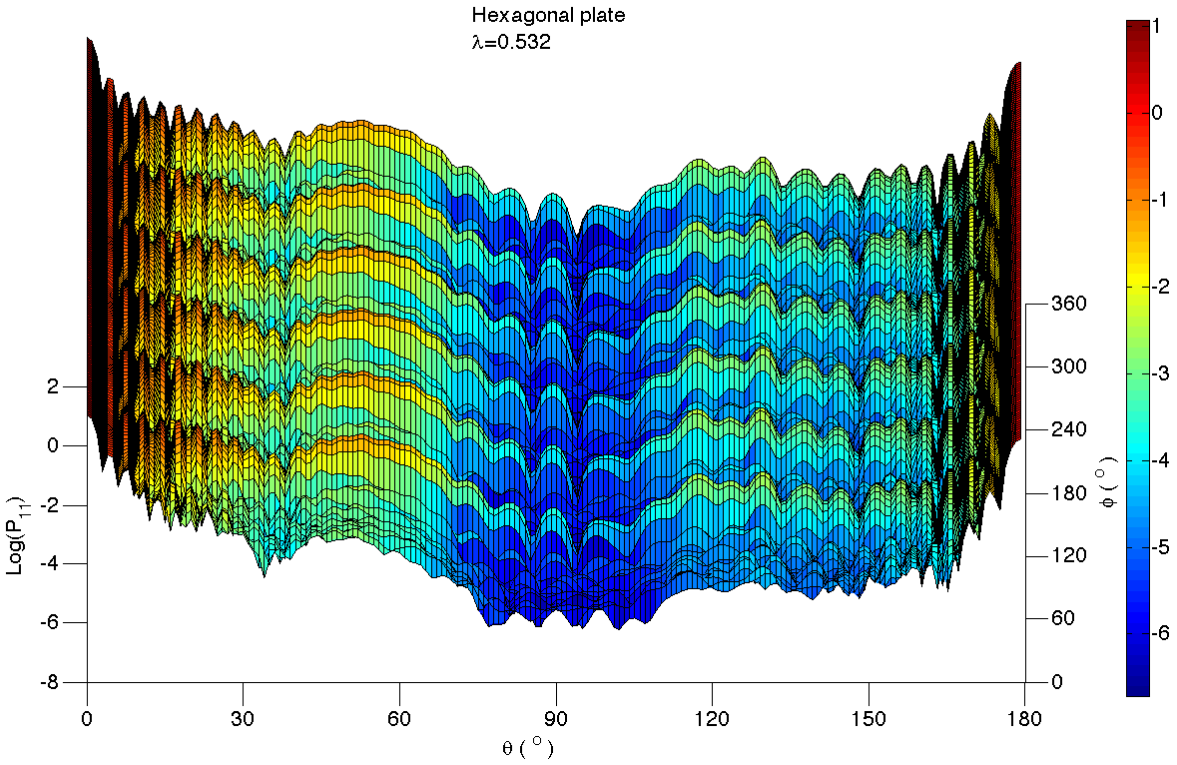

Fig. 12. The phase matrix element P_{11} of the horizontally oriented hexagonal plate with an aspect ratio of 1/3 and a semi-diameter $D = 10\mu m$. The wavelength of the incident beam $\lambda = 0.532\mu m$ and the incident angle is 0^o.

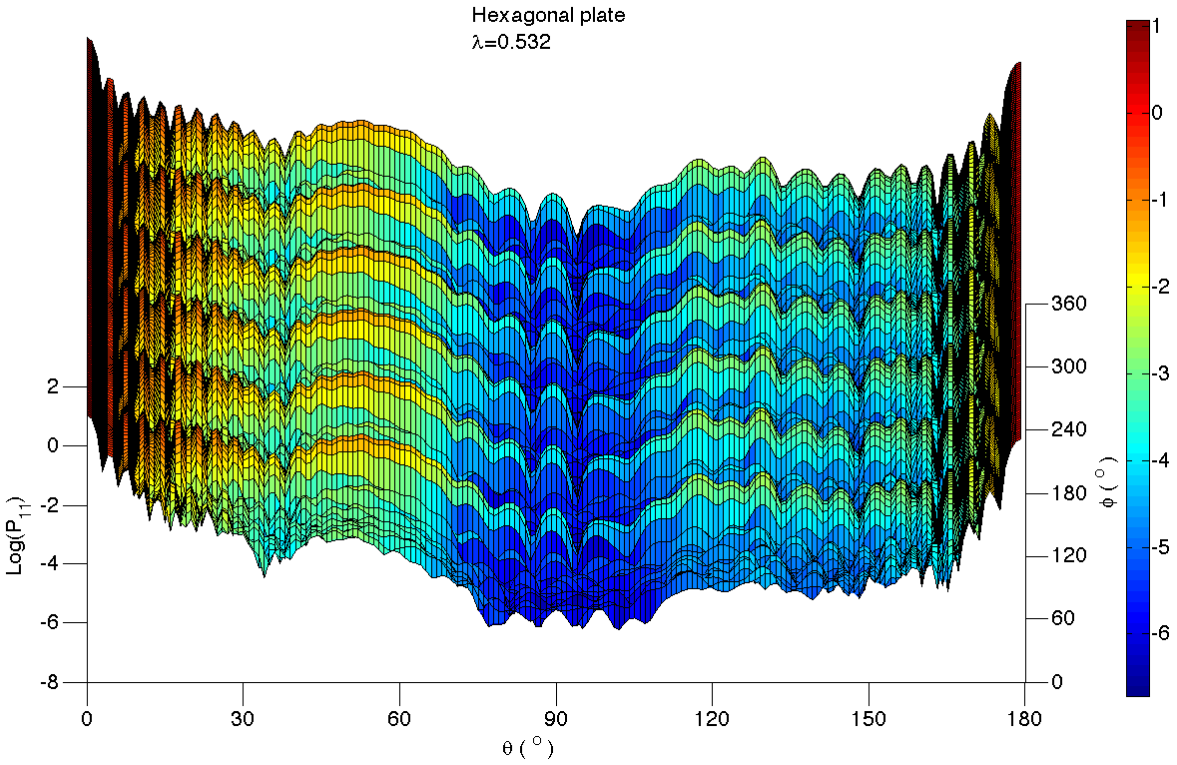

Fig. 13. The phase matrix element P_{11} of the horizontally oriented hexagonal plate with an aspect ratio of 1/3 and a semi-diameter $D = 10\mu m$. The wavelength of the incident beam $\lambda = 0.532\mu m$ and the incident angle is 3^o.

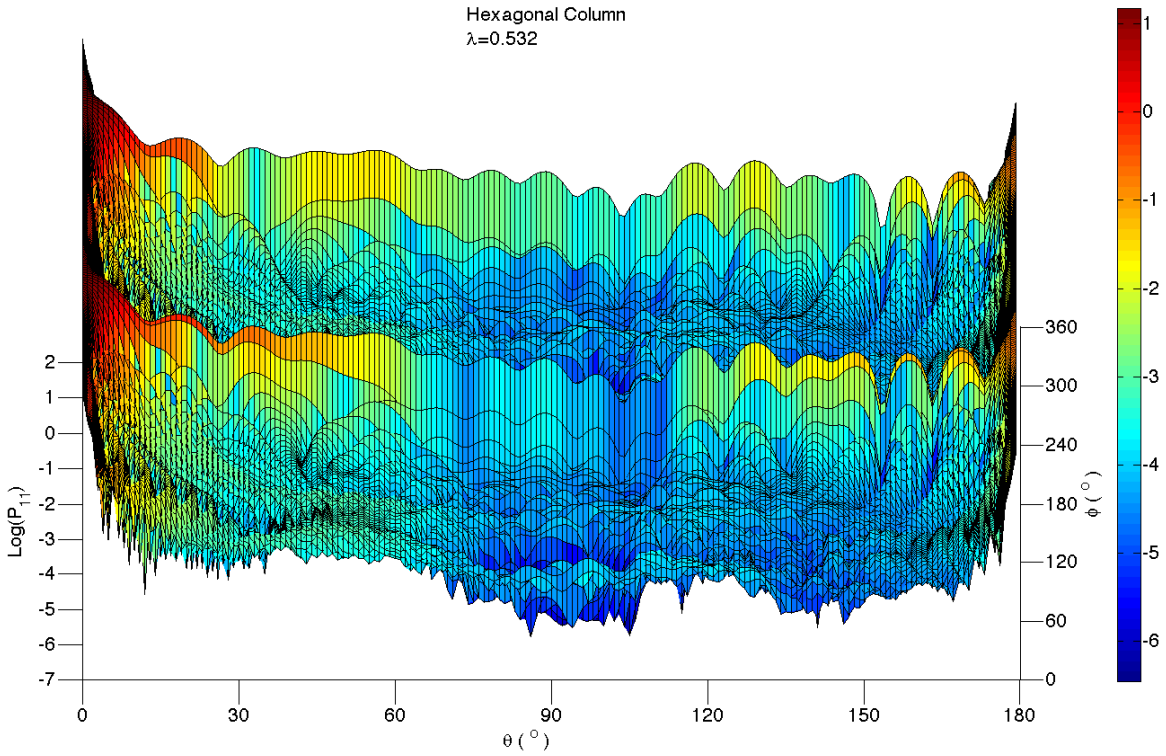

Fig. 14. The phase matrix element P_{11} of the horizontally oriented hexagonal column with an aspect ratio of 3 and a semi-diameter $D = 6\mu m$. The wavelength of the incident beam $\lambda = 0.532\mu m$ and the incident angle is 0^o.

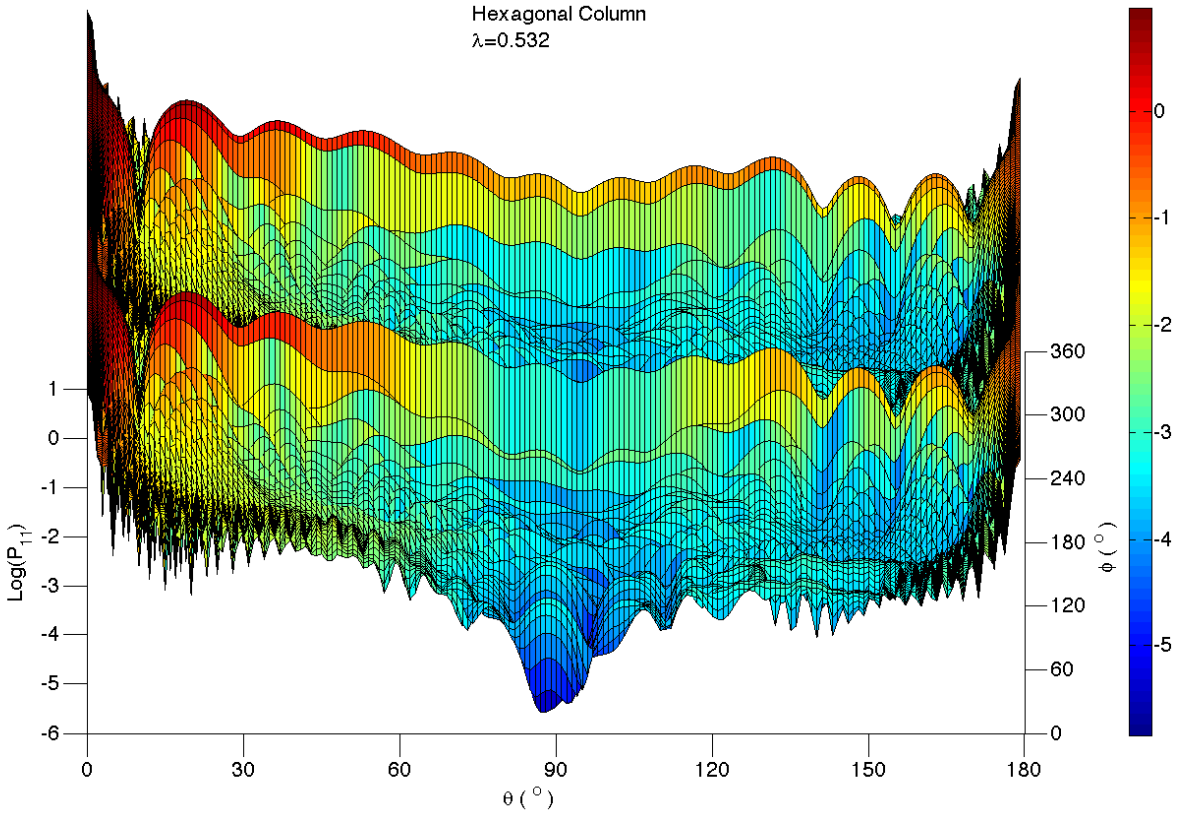

Fig. 15. The phase matrix element P_{11} of the horizontally oriented hexagonal column with an aspect ratio of 3 and a semi-diameter $D = 6\mu m$. The wavelength of the incident beam $\lambda = 0.532\mu m$ and the incident angle is 3^o.

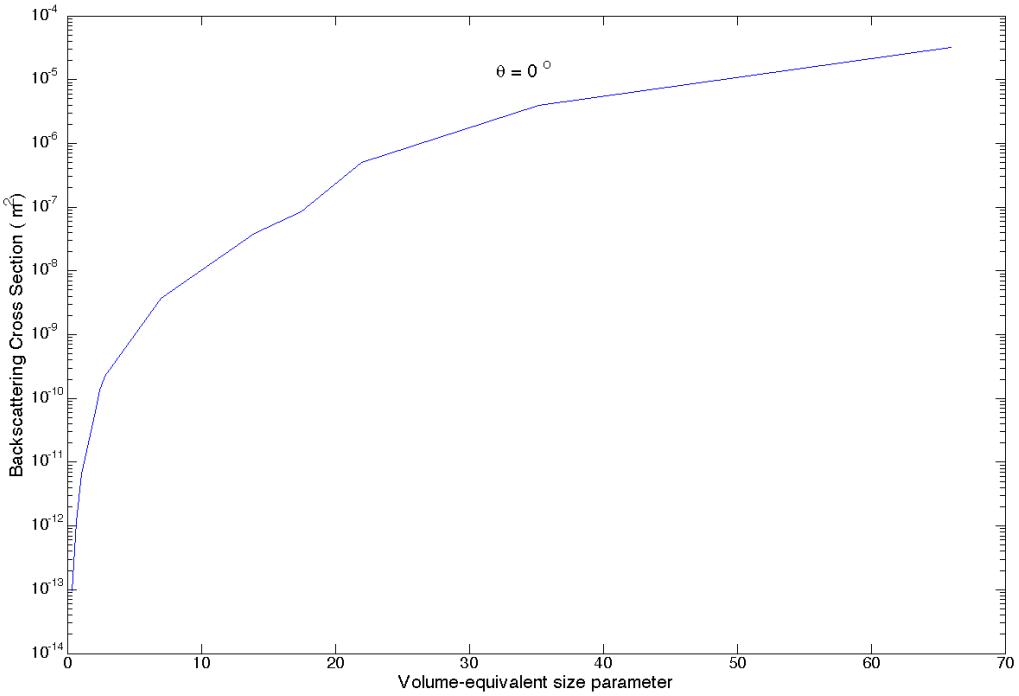

Fig. 16. The variation of backscattering cross section versus volume-equivalent size parameter for an incident angle of $\theta = 0^o$.

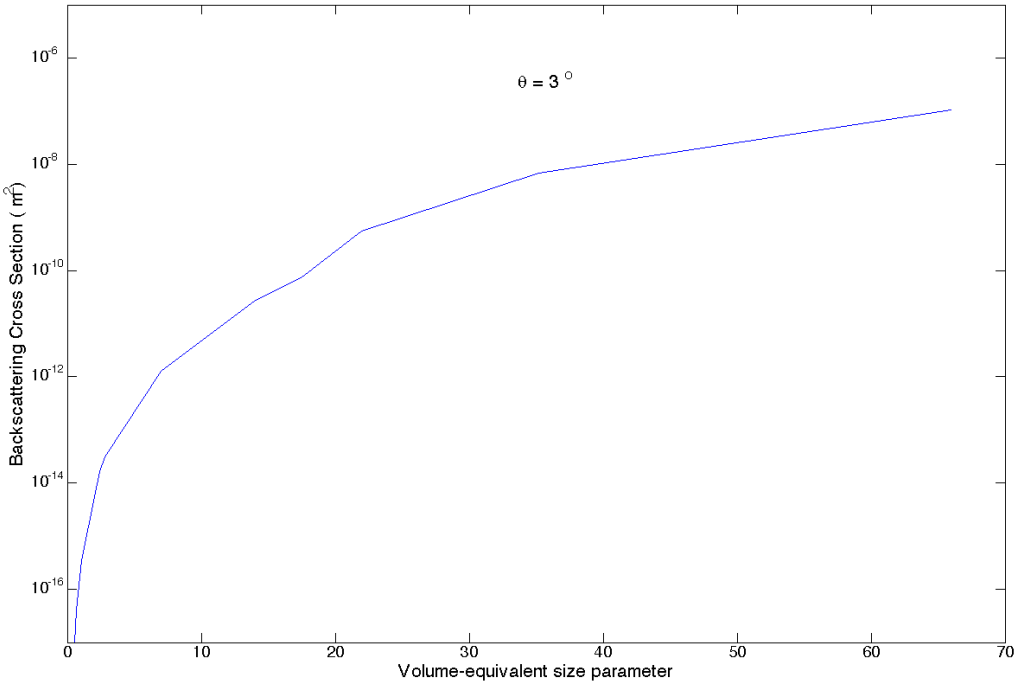

Fig. 17. The variation of backscattering cross section versus volume-equivalent size parameter for an incident angle of $\theta = 3^o$.

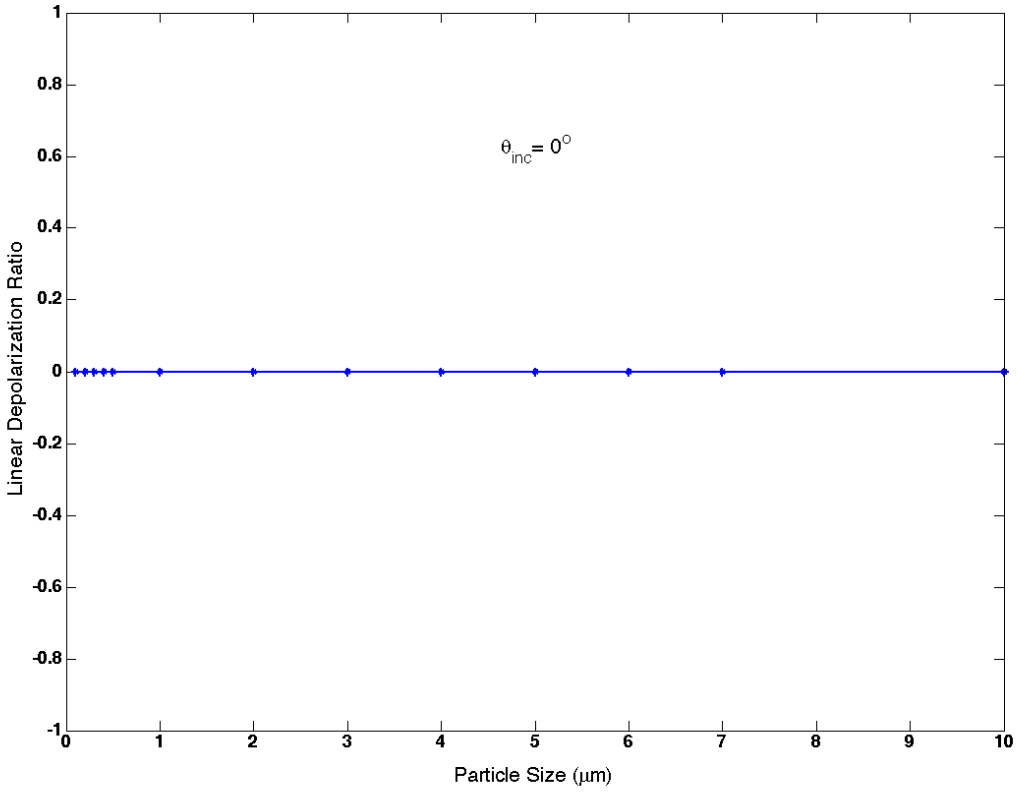

Fig. 18. The variation of the degree of linear depolarization versus volume-equivalent size parameter for an incident angle of $\theta = 0^o$.

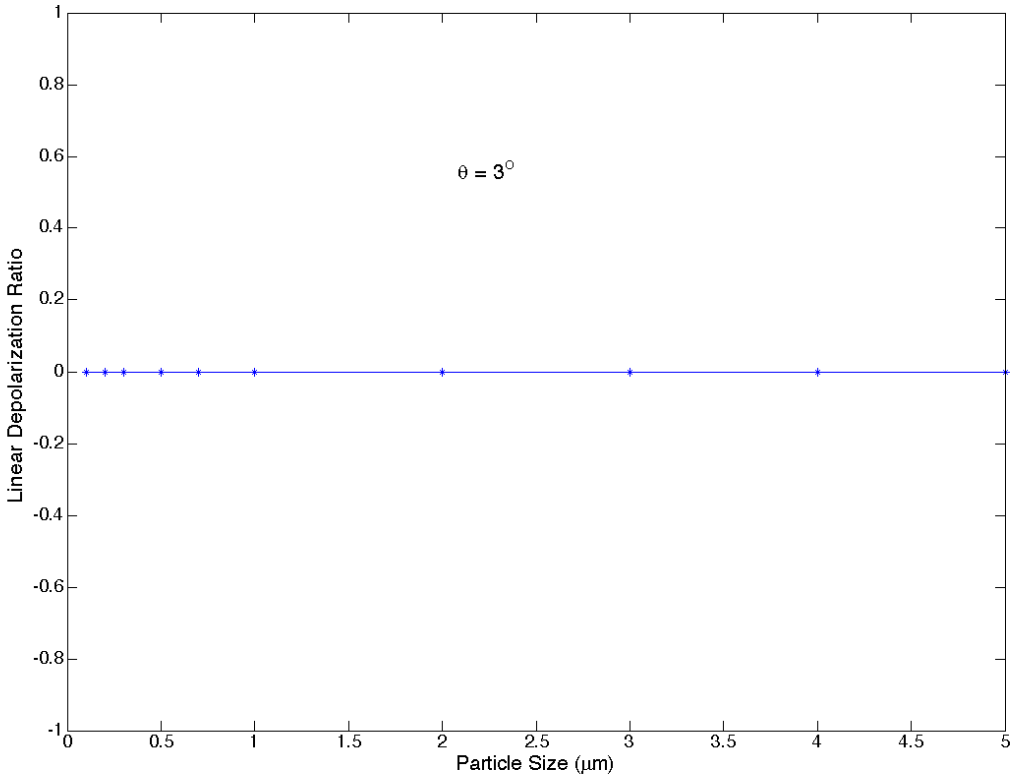

Fig. 19. The variation of the degree of linear depolarization versus volume-equivalent size parameter for incident angle $\theta = 3^o$.

CHAPTER IV

CONCLUSIONS

Lidar backscattering experiments are of great importance in detecting cloud properties. It has long been noted that the backscattering depolarization ratio can be used to determine the cloud phase. However, in order to fully interpret the data from satellites, the single-scattering properties of ice crystals such as hexagonal plates and columns must be fully understood. The conventional geometric optics ray-tracing method has limits in certain directions, particularly for direct backscattering. In this research, we studied the scattering properties of horizontally oriented hexagonal plates and columns using the DDA method. The DDA method is a powerful tool for calculating the light scattering problems associated with arbitrarily shaped particles. Our results showed that horizontally oriented hexagonal ice plates have strong backscatter and a nearly zero depolarization ratio in the zenith direction, while horizontally oriented hexagonal columns with random rotations around the particle axes have much less backscatter in the zenith angle. Thus, when determining the cloud phase using the CALIPSO data, the effect of horizontally oriented ice plates must be included to obtain more accurate results. Our current research only investigated the scattering properties of the oriented hexagonal particles with size parameters around 100. In ice clouds, the size parameter of hexagonal ice plates can reach up to 10,000. The DDA method is not applicable to such large size parameters and a more advanced technique should be employed.

REFERENCES

[1] D. P Wylie, W. P. Menzel, and K. I. Strabala, "Four years of global cirrus cloud statistics using HIRS," J. Clim. **7**, 1972 $C1986$ (1994).

[2] K. N. Liou, "Influence of cirrus clouds on weather and climate processes: a global perspective," Mon. Wea Rev. **114**, 1167C 1199 (1986).

[3] E. F. Harrison, P. Minnis, B. R. Barkstrom, V. Ramanathan, R. D. Cess, and G. G. Gibson, "Seasonal variation of cloud radiative forcing derived from the Earth radiation budget experiment," J. Geophys. Res. **95**(D11), 18,687−18,703 (1990).

[4] K. Sassen, "Advances in polarization diversity lidar for cloud remote sensing," Proc. IEEE, Remote Sensing Instruments for Environmental Research **82**, pp.1907−1914 (1994).

[5] D. M. Winker, J. Pelon, and M. P. McCormick, "The CALIPSO mission: spaceborne lidar for observation of aerosols and clouds," Proc. SPIE **4893**,1−11. (2003).

[6] Y. Hu, Z. Liu, D. Winker, M. Vaughan, and V. Noel, "Simple relation between lidar multiple scattering and depolarization for water clouds," Opt. Lett. **31**, 1809−1811 (2006).

[7] Y. Hu, 2007. "Depolarization ratio-effective lidar ratio relation: theoretical basis for space lidar cloud phase discrimination," Geophys. Res. Lett. **34** (2007), doi:10.1029/2007/GL029584.

[8] Y. Hu, M. Vaughan, Z. Liu, B. Lin, P. Yang, D. Flittner, B. Hunt, R. Kuehn, J. Huang, D. Wu, S. Rodier, K. Powell, C. Trepte, and D. Winker, "The depo-

larization C attenuated backscatter relation: CALIPSO lidar measurements vs. theory," Opt. Exp. **15**, 5327−5332 (2007).

[9] H.-M Cho, P. Yang, G. W. Kattawar, S. L. Nasiri, Y. Hu, P. Minnis, C. Tepte, and D. Winker, "Depolarization ratio and attenuated backscatter for nine cloud types: analyses based on collocated CALIPSO lidar and MODIS measurements," Opt. Exp. **16**, 3931−3948 (2008).

[10] W. L. Eberhard, "Cirrus properties deduced from CO_2 lidar observations of zenith -enhanced backscatter from oriented crystals, in fire cirrus cloud results," NASA Conf. Publ. **3228**, pp. 9−12 (1993).

[11] M. I. Mishchenko and K. Sassen, "Depolarization of lidar returns by small ice crystals: an application to contrails," Geophys. Res. Lett. **25**, 309−312 (1998).

[12] K. Sassen, "The polarization lidar technique for cloud research: a review and current assessment," Bull. Am. Meteorol. Soc. **72**, 1848−1866 (1991).

[13] R. M. Schotland, K. Sassen, and R. Stone, "Observations by lidar of linear depolarization ratios by hydrometeors," J. Appl. Meteor. **10**, 1011−1017 (1971).

[14] V. Noel, H. Chepfer, "Study of ice crystal orientation in cirrus clouds based on satellite polarized radiance measurements," J. Atmos. Sc. **61**(16), 2073−2081 (2004).

[15] M. I. Mishchenko, L. D. Travis, D. W. Mackowski, "T-matrix computations of light scattering by nonspherical particles: a review," J. Quant. Spectrosc. Radiat. Transfer **55**, 535−575 (1996).

[16] P. Yang, Y. X. Hu, D. M. Winker, J. Zhao, C. A. Hosteller, B. A. Baum, M. I. Mishchenko, and J. Reichardt, "Enhanced lidar backscattering by horizontally

oriented ice plates," J. Quant. Spectrosc. Radiat. Transfer **79-80**, 1139−1157 (2003).

[17] E. M. Purcell , C. R. Pennypacker, "Scattering and adsorption of light by nonspherical dielectric grains," Astrophys. J. **186**, 705−714 (1973).

[18] G. H. Goedecke, S. G. O'Brien, "Scattering by irregular inhomogeneous particles via the digitized Green's function algorithm," Appl. Opt. **27**, 2431−2438 (1988).

[19] B. T. Draine, "The discrete-dipole approximation and its application to interstellar graphite grains," Astrophys. J. **333**, 848−872 (1988).

[20] B. T. Draine, J. J. Goodman, "Beyond clausius-mossotti - wave-propagation on a polarizable point lattice and the discrete dipole approximation," Astrophys. J. **405**, 685-697 (1993).

[21] B. T. Draine, P. J. Flatau, "Discrete-dipole approximation for scattering calculations," J. Opt. Soc. Am. A **11**, 1491−1499 (1994).

[22] B. T. Draine, "The discrete dipole approximation for light scattering by irregular targets," in Light Scattering by Nonspherical Particles, Theory, Measurements, and Applications, M. I. Mishchenko, J. W. Hovenier, L. D. Travis, eds. (Academic Press), pp.131−145.

[23] M.A. Yurkin and A.G. Hoekstra, "The discrete dipole approximation: an overview and recent developments," J. Quant. Spectr. Rad. Transf. **106**, 558−589 (2007).

[24] M. A. Yurkin, V. P. Maltsev, A. G. Hoekstra, "The discrete dipole approximation for simulation of light scattering by particles much larger than the wavelength," J. Quant. Spectrosc. Radiat. Transfer **106**, 546−557 (2007).

[25] M.A. Yurkin, "Current capabilities of the discrete dipole approximation for very large particles: speed, accuracy, and computational tricks", presented at Proceedings of the DDA - Workshop, Institut für Werkstofftechnik, Bremen, Germany, March 2007.

[26] P. C. Waterman, "The T-matrix revisited," J. Opt. Soc. Am. **A 24**, 2257−2267 (2007).

[27] C. Yeh, S. Colak, P. W. Barber, "Scattering of sharply focused beams by arbitrarily shaped dielectric particles: an exact solution," Appl. Opt. **21**, 4426−4433 (1982).

[28] M. I. Mishchenko, D. J. Wielaard, B. E. Carlson, "T-matrix computations of zenith-enhanced lidar backscatter from horizontally oriented ice plates," Geophys. Res. Lett. **24**, 771−774 (1997).

[29] A. Ono, "The shape and riming properties of ice crystals in natural clouds," J. Atmos. Sci. **26**, 138−147 (1969).

[30] A. J. Heymsfield, C.M.R. Platt, "A parameterization of the particle size spectrum of ice clouds in terms of the ambient temperature and ice water content," J. Atmos. Sci. **41**, 846−855 (1984).

VITA

Feng Zhang received his Bachelor of Science degree in physics at Nankai University in 1999 and Master of Science degree in physics in 2002. He then studied in the Department of Physics at Texas A&M University and received a Master of Science degree in 2007. After that he moved to the Department of Atmospheric Sciences at Texas A&M University and received his Master of Science degree in August 2009. He may be reached at the Department of Atmospheric Sciences, Texas A&M University, 3150 TAMU, College Station, TX77843. His email address is fengzhang@tamu.edu.